Naval Research Laboratory
Washington, DC 20375-5320

NRL/MR/5670--04-8779

Comparison of the Frequency Response and Voltage Tuning Characteristics of a FFP and a MEMS Fiber Optic Tunable Filter

FRANK BUCHOLTZ
Consultant
Crofton, MD

MARK SEAVER
Optical Techniques Branch
Optical Sciences Division

MICHAEL D. TODD
University of California
La Jolla, CA

May 12, 2004

REPORT DOCUMENTATION PAGE

Form Approved
OMB No. 0704-0188

1. REPORT DATE *(DD-MM-YYYY)*	2. REPORT TYPE	3. DATES COVERED *(From - To)*
12 May 2004	Memorandum report	

4. TITLE AND SUBTITLE

Comparison of the Frequency Response and Voltage Tuning Characteristics of a FFP and a MEMS Fiber Optic Tunable Filter

5a. CONTRACT NUMBER

5b. GRANT NUMBER

5c. PROGRAM ELEMENT NUMBER

6. AUTHOR(S)

Frank Bucholtz,* Mark Seaver, and Michael D. Todd†

5d. PROJECT NUMBER

5e. TASK NUMBER

5f. WORK UNIT NUMBER

7. PERFORMING ORGANIZATION NAME(S) AND ADDRESS(ES)

Naval Research Laboratory, Code 5670
4555 Overlook Avenue, SW
Washington, DC 20375-5320

8. PERFORMING ORGANIZATION REPORT NUMBER

NRL/MR/5670--04-8779

9. SPONSORING / MONITORING AGENCY NAME(S) AND ADDRESS(ES)

Naval Research Laboratory
4555 Overlook Avenue, SW
Washington, DC 20375-5320

Office of Naval Research
800 North Quincy Street, Code 621114n
Arlington, VA 22217

10. SPONSOR / MONITOR'S ACRONYM(S)

11. SPONSOR / MONITOR'S REPORT NUMBER(S)

12. DISTRIBUTION / AVAILABILITY STATEMENT

Approved for public release; distribution is unlimited.

13. SUPPLEMENTARY NOTES

*Consultant, Crofton, MD 21114
†Current address: University of California, San Diego, Department of Structural Engineering, La Jolla, CA 92093

14. ABSTRACT

Tunable optical filters based on a Fabry-Perot element are a critical component in many wavelength based fiber optic sensor systems. This report compares the performance of two fiber-pigtailed tunable optical filters, the fiber Fabry-Perot (FFP) filter from Micron Optics and a recently developed type of tunable filter based on Micro Electro-Mechanical System (MEMS) technology from Nortel. The findings indicate that while both filters have similar bandpass characteristics, the FFP scans one free spectral range with a linear 0-10 volt signal while the MEMS system displays a voltage squared response and requires up to 35 volts to scan one free spectral range. The small signal response of both filters suggests that they can operate at frequencies up to 20 kHz and possibly as high as 100 kHz.

15. SUBJECT TERMS

Tunable Fabry-Perot filters; MEMS; Voltage response; Frequency response; Bandwidth; Fiber optic sensors

16. SECURITY CLASSIFICATION OF:			17. LIMITATION OF ABSTRACT	18. NUMBER OF PAGES	19a. NAME OF RESPONSIBLE PERSON
a. REPORT	b. ABSTRACT	c. THIS PAGE			Mark Seaver
Unclassified	Unclassified	Unclassified	UL	27	19b. TELEPHONE NUMBER *(include area code)* (202) 767-3590

Standard Form 298 (Rev. 8-98)
Prescribed by ANSI Std. Z39.18

CONTENTS

COMPARISON OF THE FREQUENCY RESPONSE AND VOLTAGE TUNING CHARACTERISTICS OF A FFP AND A MEMS FIBER OPTIC TUNABLE FILTER

1. Background

Fiber optic sensor arrays based on fiber Bragg gratings (FBGs) have proven to be viable, accurate systems for mechanical modal analysis [Tod01], direct load monitoring [Ten01,Wan01], and nonlinear dynamics for structural health monitoring [Mon03,Nic03a,Nic03b]. Briefly, FBGs operate as mechanical strain sensors by transforming change in length into a change in the optical wavelength of light reflected from the sensor. Hence, the interrogation of an array of such sensors requires a wavelength discriminator both to distinguish one sensor in the array from all others and to measure the change in wavelength of the light from any particular sensor.

To provide wavelength discrimination, interrogation techniques based on tunable optical filters have been developed [Ker97] . Thus far, the tunable filter most widely used in this application is a fiber-pigtailed tunable Fabry-Perot filter known as the fiber Fabry-Perot (FFP) filter [Sto87]. This filter employs a piezoelectric element to vary the gap between two optical reflectors forming a Fabry-Perot cavity. However, as the bandwidth requirements of sensor arrays increase, the frequency response of the piezo-element in the FFP can becomes the bandwidth-limiting component. Recently, a new type of fiber-pigtailed, voltage-tunable Fabry-Perot filter, based on MEMS (Micro Electro-Mechanical System) technology has been introduced having potentially higher bandwidth. The new filter also comprises a Fabry-Perot cavity, or etalon, but here the cavity length is varied by the movement of a thin diaphragm containing an optical reflector [Jer91, Lar95].

The purpose of this report is to compare the frequency response and voltage tuning characteristics of these two types of fiber-coupled filters. The results will be useful for the design of optical interrogation systems for FBG sensor arrays. The reader is cautioned that these results are preliminary in the sense that only two particular filters were compared and an extrapolation to general behavior is only as good as the reproducibility of the manufacturing process employed by the vendors of each filter.

2. Introduction

In this report we summarize the results of preliminary tests of the frequency response and voltage tuning characteristics of two types of fiber-coupled voltage-tunable wavelength-

Manuscript approved March 25, 2004

selective filters - the FFP filter and the MEMs filter. Both filters are based on a Fabry-Perot etalon to provide wavelength selectability. The fundamental operation of a Fabry-Perot filter is shown in **Fig. 1**. This filter is treated in detail in the literature [Sal91, Bor99] where it is also referred to as a resonator. For spacing d between the reflectors, light is transmitted through the resonator only in the vicinity of discrete frequencies given by

$$\nu_m = m(c/n)(1/2d) \qquad m = 1,2,.... \tag{1}$$

where c = speed of light in vacuum, m = integer (referred to as the "mode order"), and n is the index of refraction of the medium between the reflectors. Resonance modes exist at frequencies such that an integer number of optical wavelengths are contained in the "round-trip" optical length 2dn of the cavity of physical length d. Hereafter, we assume the etalon gap is air so that n = 1. For fixed d, the spacing in frequency between adjacent modes is constant and is given by

$$(\nu_{m+1} - \nu_m) \equiv \nu_{fsr} = c/2d, \tag{2}$$

a quantity called the free spectral range (FSR) of the resonator. The wavelengths of the resonator modes are easily calculated

$$\lambda_m = \frac{c}{\upsilon_m} = \frac{2d}{m} \tag{3}$$

and we see that the wavelength spacing between adjacent modes depends is not constant but depends on the mode order (see **Fig. 1(c)**)

$$(\lambda_m - \lambda_{m+1}) = 2d\left(\frac{1}{m} - \frac{1}{m+1}\right) \tag{4}$$

Let P_i be the optical power entering the cavity and let P_t be the optical power transmitted by the cavity. By summing the electric fields of the light exiting the cavity from all the partial transmissions and reflections between the mirrors, the transmittance $T = (P_t / P_i)$ is found to be [Sal91]

$$T = \frac{P_t}{P_i} = \frac{T_{\max}}{1 + (2F/\pi)^2 \sin(\pi\nu/\nu_{fsr})} \tag{5}$$

where

$$T_{\max} = \frac{|t|^2}{(1-r)^2}, \qquad t = t_1 t_2, \qquad r = r_1 r_2 \tag{6}$$

t_i is the transmittance of the i^{th} reflector, r_i is the reflectance of the i^{th} reflector, and where the finesse

$$F = \frac{\pi r^{1/2}}{1-r}. \tag{7}$$

The full width at half maximum (FWHM) of the resonance peaks is thus given by

$$FWHM = \nu_{fsr} / F. \tag{8}$$

A Fabry-Perot cavity can function as a spectrum analyzer by changing the mirror spacing d a small amount Δd using, for example, a piezoelectric element. Here, although the free spectral range changes by a relatively small amount

$$\Delta\nu_{fsr} = -\nu_{fsr}(\Delta d/d), \tag{9}$$

the m^{th} resonance frequency changes by

$$\Delta\nu_m = -\nu_m(\Delta d/d) = -m\nu_{fsr}(\Delta d/d), \tag{10}$$

an amount m times larger than the change in the FSR! By choosing a cavity length such that the optical wavelength range of interest corresponds to a relatively large m value, say m = 10 - 1000, a small change in cavity length can produce a relatively large change in the frequency corresponding to the m^{th} resonance. It is then possible for the m^{th} mode to

traverse a frequency range equivalent to a full free-spectral range or more with a relatively modest change in voltage. Hence, the cavity acts in transmission as a voltage-tunable optical filter and, as such, can operate as a spectrum analyzer by sweeping predictably and repeatedly through a range of optical wavelengths.

Assume the cavity length change Δd corresponds to a voltage change ΔV applied to a piezoelectric element and define

$$\beta = \Delta d / \Delta V. \tag{11}$$

Then

$$\Delta \nu_m / \Delta V = -\nu_m \beta / d. \tag{12}$$

Example: Typical values for a commercially available FFP filter are FSR= 9400 GHz, and $\Delta \nu_m / \Delta V = -(\textit{One full FSR for } \Delta V = 12V)$. The resonance corresponding to λ_m=1550 nm wavelength has order m = c/(λ_m*FSR) ~ 20, the etalon spacing (assuming air in the gap) is d = c / (2*FSR) = 16 um, and the sensitivity of the gap length to voltage change is β = 0.06 um/V.

For the PZT element used in the FFP, the cavity length depends linearly on voltage since the strain *e* in a piezoelectric material is related to the applied voltage V by

$$e = d_{ij} E = d_{ij} (V / t), \tag{13}$$

where d_{ij} (m/V) is the piezoelectric strain coefficient relating strain in the i-direction to the electric field E in the j-direction, t is the thickness of the PZT material to which the voltage is applied (not the gap length). For a MEMS device, the cavity length results from the gap between a thin membrane and a substrate. Electrically, the two surfaces form a capacitor where the electrostatic force between the two "plates" due to an applied voltage V is [Jer91, Lar95]

$$F = \left(\frac{A \varepsilon_o}{2} \right) \frac{V^2}{x^2} \tag{14}$$

where x is the distance between the electrodes (not the gap length!), A is the total electrode area, and ε_0 is the permittivity of air. Given a mechanical stiffness 1/k for the MEMS diaphragm, the gap length - and therefore the center wavelength - depends quadratically on the applied voltage.

$$d = \frac{F}{k} = \left(\frac{A\varepsilon_o}{2kx^2}\right)V^2 \tag{15}$$

3. Filter Measurements

The two filters compared for the purposes of this report were a Micron Optics (Atlanta, GA) FFP-TF filter and a CoreTek (currently a subsidiary of Nortel Networks) MT-15 MEM filter. Examples of the engineering designs of these devices, based on the patent literature, are shown in **Fig. 2**. The specific designs used in the actual devices tested here is not known.

3.A. Source Characterization

Broadband sources were required for the wavelength versus voltage measurement and two types of sources were used to cover the desired wavelength range. The short wavelength portion of the range was illuminated using an amplified spontaneous emission (ASE) source (BT&D Technologies, EFA3000 Series, Er-doped fiber amplifier(EDFA)), and the long wavelength range was illuminated using a superluminescent light-emitting diode or SLED (Opto Speed SA, SLED1550D10A).

For both sources we also measured the degree-of-polarization (DOP) using an HP-8509B Polarization Analyzer.

The optical spectrum of the SLED source is shown in **Fig. 3.** The spectral shape is nearly Gaussian with FWHM of approximately 40 nm, between 1555-95 nm, and with 65% DOP owing to the superluminescent nature of the device. The optical spectrum of the ASE source in **Fig. 4** has width at half maximum power of, again, approximately 40 nm, but in the wavelength range 1525 - 1565 nm and the DOP is less than 2% at the largest pump power (375 mA). The spectral shape of the ASE is due to the absorption spectrum of the Er ions in the silica glass matrix. The EDFA comprising the ASE source

can also be used as an optical amplifier for the SLED source. The spectra corresponding to this arrangement are shown in **Fig. 5.** In addition, the EDFA effectively depolarizes the SLED. The DOP of the amplified SLED source decreases from 65% for no amplification to 8.4% at the largest amplification (pump current 375 mA). The SLED spectrum effectively "pulls" the ASE spectrum to longer wavelengths, closer to the center wavelength of the SLED.

3.B. Wavelength vs Voltage

The experimental arrangement used to measure the voltage tuning characteristics of the FFP filter is shown in **Fig. 6**. Adjustable DC voltage was provided by an HP6236B power supply attached directly to the input leads of the FFP and monitored with a Fluke handheld voltmeter. The optical input to the FFP consisted of either the SLED source or the ASE source - to cover the full wavelength range - and the output of the FFP was monitored using an optical spectrum analyzer (OSA) (Anritsu MS9710B). The result of the measurement in **Fig. 7** shows a tuning coefficient and FSR of approximately 5.7 nm/V and 65 nm, respectively. The wavelength tuning curve is seen to contain both nonlinearity and hysteresis, two nonideal characteristics that can adversely affect the frequency response of the device.

The tuning characteristics of the MEMs filter was measured using the same set-up as in **Fig. 6** and the result is shown in **Fig. 8**. As discussed above, the tuning curve is largely quadratic first order but does contain both linear and higher order terms as seen in the curve fit shown in the inset. However, in contrast to the FFP device, the response exhibits extremely low hysteresis suggesting that the frequency response characteristics of the MEMs device will be superior.

A comparison of the wavelength tuning coefficient ($d\lambda/dV$) is shown in **Fig. 9**.

3.C. Small Signal Frequency Response

A path-unbalanced interferometer (**Fig. 10**) was used to monitor the wavelength modulation of the light transmitted through the filter in response to voltage modulation.

Given an interferometer with physical path imbalance L, the phase difference between the light traveling in the two arms of the interferometer at the point where they recombine in the second coupler is

$$\phi = \frac{2\pi nL}{\lambda} \tag{16}$$

where n is the index of refraction of the fiber core and λ is the optical wavelength. The change in phase due to change in wavelength is given by

$$\delta\phi = -\frac{2\pi nL}{\lambda^2}\delta\lambda \tag{17}$$

or, in terms of voltage sensitivity (dλ/dV) and voltage change δV,

$$\delta\phi = -\frac{2\pi nL}{\lambda^2}\left(\frac{d\lambda}{dV}\right)\delta V \tag{18}$$

Experimentally, a reasonable phase shift to observe without difficulty is, say, 300 mrad, pp. Using (dλ/dV) = -2 nm/V, a value near the middle of the MEMS tuning characteristic, and assuming δV = 1 mV pp, δϕ = 300 mrad pp at λ = 1550nm requires L = 4 cm. An interferometer having L = 10 cm was assembled for this measurement. Note that the relatively low value δV = 1 mV pp was chosen in anticipation of (dλ/dV) decreasing significantly with frequency.

In order to obtain an interferometer output with good fringe visibility, the coherence length of the source must not be significantly smaller than the path imbalance of the interferometer [Fra66]. In our system, the coherence length L_{coh} is determined by the FWHM Δλ of the tunable filter

$$L_{coh} = \lambda^2/\Delta\lambda \tag{19}$$

The output spectrum of each filter is shown in **Fig. 11** . The table below summarizes the measured FWHM and the calculated coherence length at λ = 1550 nm for each filter. We

conclude that "good enough" fringe visibility should be obtained for either filter with L = 10 cm path imbalance.

Table 1: Center wavelength, spectral width, and coherence light of light transmitted by the two optical filters.

Device	Center Wavelength* (nm)	FWHM (nm)	Coherence Length (cm)
MEMS	1574.9	0.1	2.4
FFP	1562.6	0.2	1.2

At given fixed applied bias voltage (See **Fig. 11).*

The actual system used to make the small-signal frequency response measurements is shown in **Fig. 12** and the results are shown in **Fig. 13**. The MEMS device exhibited a weak resonance near 660 kHz but otherwise showed a smooth decrease in voltage sensitivity with increasing frequency. The FFP device exhibited a strong mechanical resonance at 124 kHz followed by a sharp decrease in sensitivity. As an additional qualitative point, for all frequencies but especially below resonance, the FFP device exhibited significantly more harmonic distortion than the MEMS device.

The following two tables summarize the technical characteristics of the devices and the "pros-and-cons" of the devices from a sensor system perspective.

Table 2: Technical comparison of the two filters.

Parameter	MEMS	FFP
FSR @ 1550 nm	140	65
"Static" $d\lambda/dV$ (nm/V)	0 – 5 (bias voltage dependent)	5.7
Max Voltage (V)	40	12
Max dc tuning range (nm)	~ 80	~ 65
Voltage Response	Quadratic ~ V^2	Linear ~ V
Spectral Passband (nm)	0.1	0.2
Frequency Response (kHz)	> 100	> 100
Drift	Low-Med	Med-High
Hysteresis	Low	Med
Harmonic Distortion	Low	High
Electro-mechanical Loading	Low	High
Electro-mechanical Resonance (kHz)	660 (weak)	50 (weak) 124 (strong)
Cost ($k)	~ 5	~ 5
Vendor	Nortel (Core Tek)	Micron Optics

Table 3: Qualitative comparison of the two filters.

Device	PRO	CON
FFP	Mostly linear voltage response	High drift
	Reliable vendor	Medium hysteresis
		High harmonic distortion
MEMS	Low hysteresis	Quadratic voltage response (Wavelength-dependent voltage sensitivity)
	Low drift	Unreliable vendor for small quantities
	Low harmonic distortion	

4. Summary

For applications requiring modulation of an optical filter at high audio to ultrasonic frequencies (20 kHz – 1 MHz), the MEMS device will offer superior performance in terms of low harmonic distortion, low hysteresis and drift. However, these advantages may be offset by the intrinsic quadratic nature of the voltage response – a nonlinearity that can be compensated in the drive electronics at the cost of increased cost and complexity and, therefore, decreased reliability. Also note that the long-term stability of MEMS devices has not been firmly established. By comparison, the PZT-based FFP provides advantages of availability and linearity of voltage sensitivity but possesses the disadvantages of drift, hysteresis and distortion.

5. References

Ath81	P.D. Atherton, N.K. Reay, J. Ring, and T.R. Hicks,"Tunable Fabry-Perot filters," Opt. Eng. **20** (6) 806-814 (1981).
Bor99	M. Born and E. Wolf, Principles of Optics, Cambridge University Press, Cambridge, 7th ed. 1999.
Dav98	Davis, Michael A., Kersey, Alan D., Bellmore, David G., "Fiber Bragg grating interrogation system with adaptive calibration," US Patent 5,818,585, October 6, 1998. Assignee: United States of America as represented by the Secretary of the Navy
Fra66	M. Françon, Chap. IV in Optical Interferometery, Academic Press, New York, 1966.
Jer91	J.H. Jerman, D.J. Clift, and S.R. Mallinson, "A miniature Fabry-Perot interferometer with a corrugated silicon diaphragm support," Sensor & Actuators A, **29** 151-158 (1991).
Ker97	A.D. Kersey, M.A. Davis, H.J. Patrick, M. LeBlanc, K.P. Koo, C.G. Askins, M.A. Putnam, and E.J. Friebele, "Fiber grating sensors," J. Lightwave Technol., **15** (8) 1442-1463 August 1997.
Lar95	M.C. Larson, B. Pezeshki, and J.S. Harris, Jr., "Vertical-coupled-cavity microinterferometer on GaAs with deformable-membrane top mirror," IEEE Photon. Technol. Lett., 7(4) 382-384, April 1995.
Mil93	C.M. Miller and Jeffrey W. Miller, "Single wafered ferrule fiber Fabry-Perot filters," U.S. Patent 5,212,746, May 18, 1993, Assignee: Micron Optics, Inc.(Atlanta, GA)
Mon03	L. Moniz, J. M. Nichols, C. J. Nichols, M. Seaver, S. T. Trickey, M. D. Todd, L. M. Pecora, and L. N. Virgin, "A Multivariate, Attractor-based Approach to Structural Health Monitoring", accepted J. Sound and Vib.
Nic03a	J. M. Nichols, M. D. Todd, and M. Seaver, and L.N. Virgin, "Use of chaotic excitation and attractor property analysis in structural health monitoring", Phys. Rev. E **67**, 016209 (2003).
Nic03b	J. M. Nichols, M. D. Todd, and J. R. Wait, "Using state space predictive modeling with chaotic interrogation in detecting preload loss in a frame structure experiment", Smart Mat. Struct. **12**, 580-601 (2003).
Sal91	B.A. Saleh and M.C. Teich, Fundamentals of Photonics, Wiley, New York, 1991.
Sto87	J. Stone and L.W. Stulz, "Pigtailed high-finesse tunable fibre Fabry-Perot interferometers with large, medium and small free spectral ranges," Electron. Lett. **12** (15) 781-783 (1987)
Sto89	J. Stone and L.W. Stulz, "Optical communication systems using Fabry-Perot cavities," US Patent 4,861,136, August 29, 1989, Assignee: American Telephone and Telegraph Company; AT&T Bell Laboratories.

Tay03	P. Tayebati, "Electrically tunable fabry-perot structure utilizing a deformable multi-layer mirror and method of making the same," US Patent 6,597,490, July 22, 2003, Assignee: CoreTek, Inc. (Wilmington, MA).
Ten01	R. C. Tennyson, A. A. Mufti, S. Rizkalla, G. Tadros and B. Benmokrane, "Structural health monitoring of innovative bridges in Canada with fiber optic sensors", Smart Mater. Struct. **10**, 560–573 (2001).
Tod01	M.D. Todd, G. A. Johnson, and S. T. Vohra, "Deployment of a fiber Bragg grating-based measurement system in a structural health monitoring application", Smart Mater. Struct. **10**, 534–539 (2001).
Wan01	G. Wang, K. Pran, G. Sagvolden, G. B. Havsgard, A. E. Jensen, G. A. Johnson and S. T. Vohra, "Ship hull structure monitoring using fibre optic sensors", Smart Mater. Struct. **10**, 472–478 (2001).
Wan03	P. Wang, D. Vakhshoori, P. Tayebati, "Tunable Fabry-Perot filter and tunable vertical cavity surface emitting laser," US Patent 6,584,126, June 24, 2003, Assignee: CireTek, Inc (Wilmington, MA).

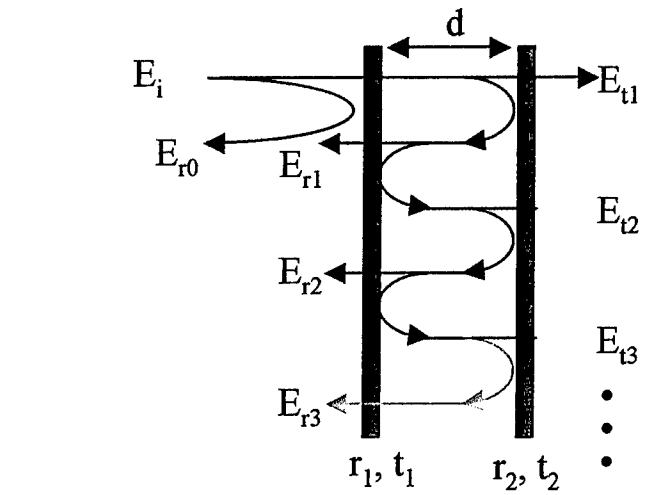

$$P_r \propto (E_{r0} + E_{r1} + E_{r2} + ...)^2 \qquad P_t \propto (E_{t1} + E_{t2} + E_{t3} + ...)^2$$

$$= P_{in} - P_t - P_{insertion\ loss} \qquad = \frac{P_{max}}{1 + (2F/\pi)^2 \sin^2(\pi\nu/\nu_F)}$$

(a)

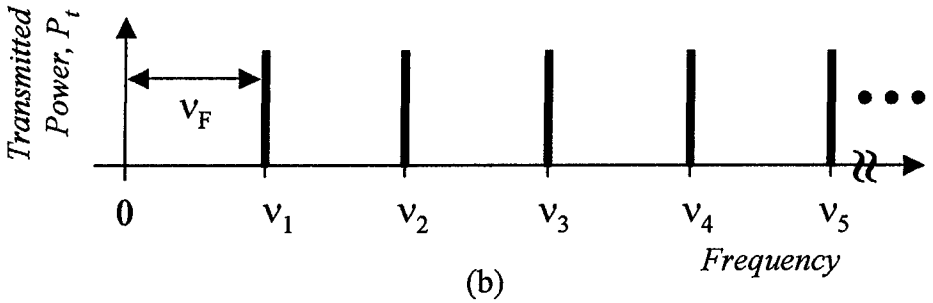

(b)

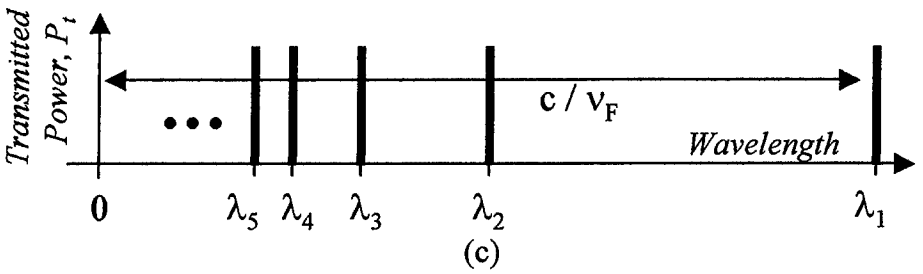

(c)

Fig. 1. *Operation of a Fabry-Perot etalon comprising two reflectors having reflectivities and transmissivities r_1 and r_2, and t_1 and t_2, respectively. (a) Optical power transmitted or reflected results from coherent addition of subbeams of light undergoing multiple reflections within the cavity. (b) Resonant modes as a function of frequency. (c) Resonant modes of the same cavity as a function of wavelength.*

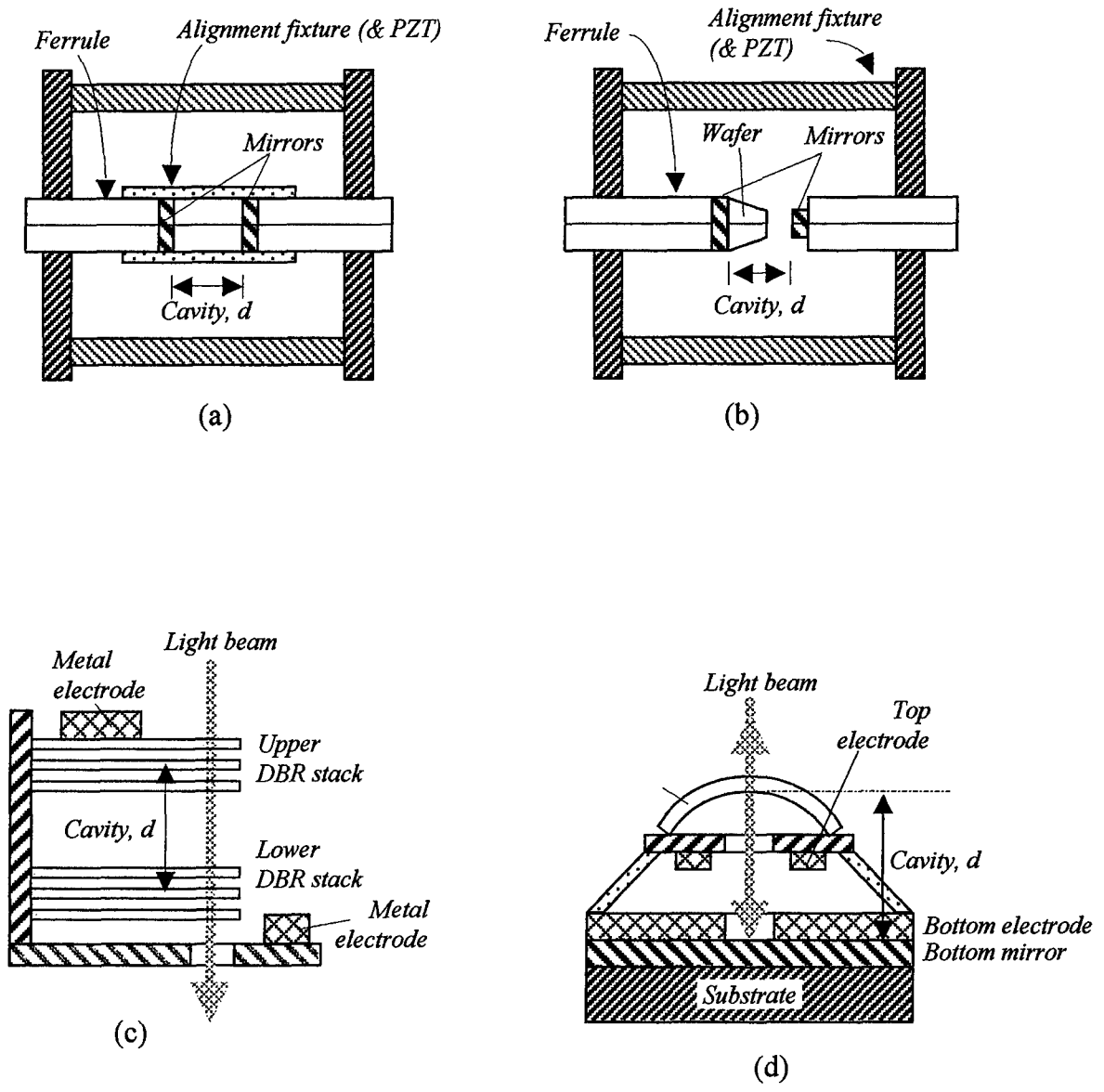

Fig. 2. *Examples of engineering designs of Fabry-Perot etalons based on (a&b) fibers in ferrule with embedded mirrors and PZT stretchers and (c&d) MEMS technology. (a) Illustration based on US patent 4,861,136. (b) Illustration based on US patent 5,212,746. (c) Illustration based on US patent 6,597,490. (d) Illustration based on US patent 6,584,126.*

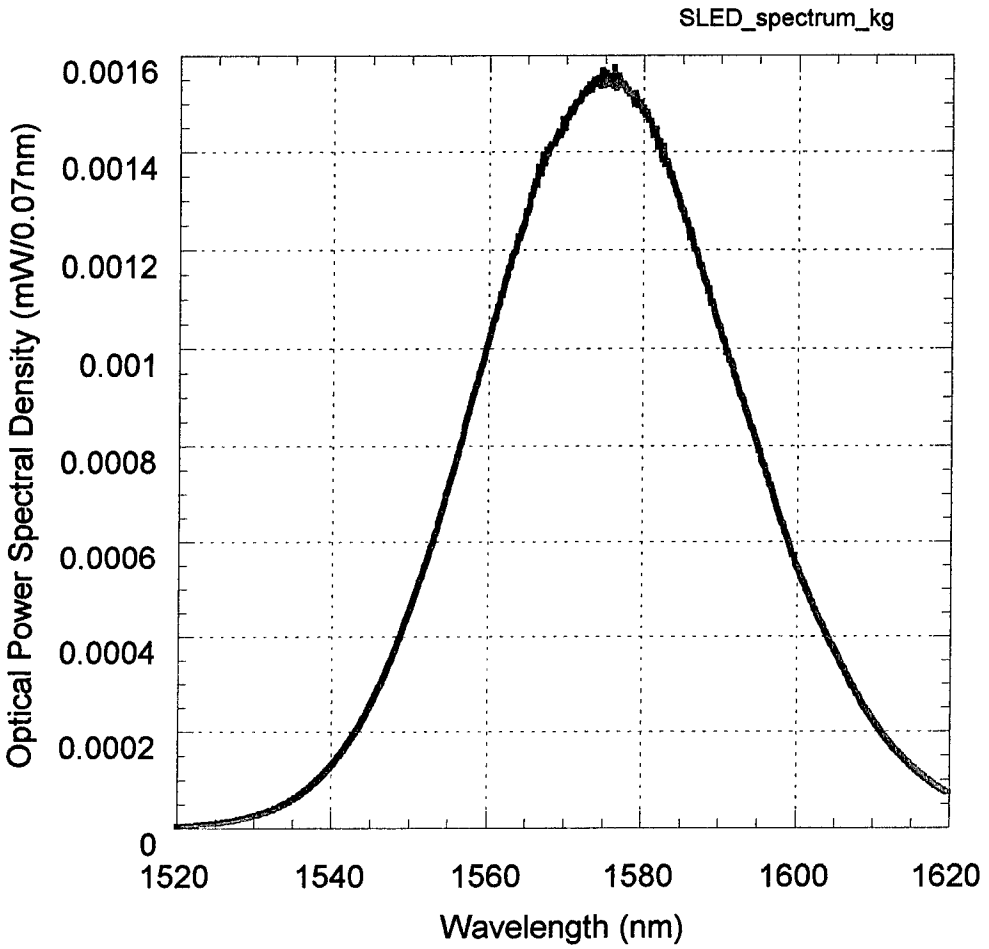

Fig. 3. *Optical spectrum of the superluminescent light-emitting diode (SLED) source.*

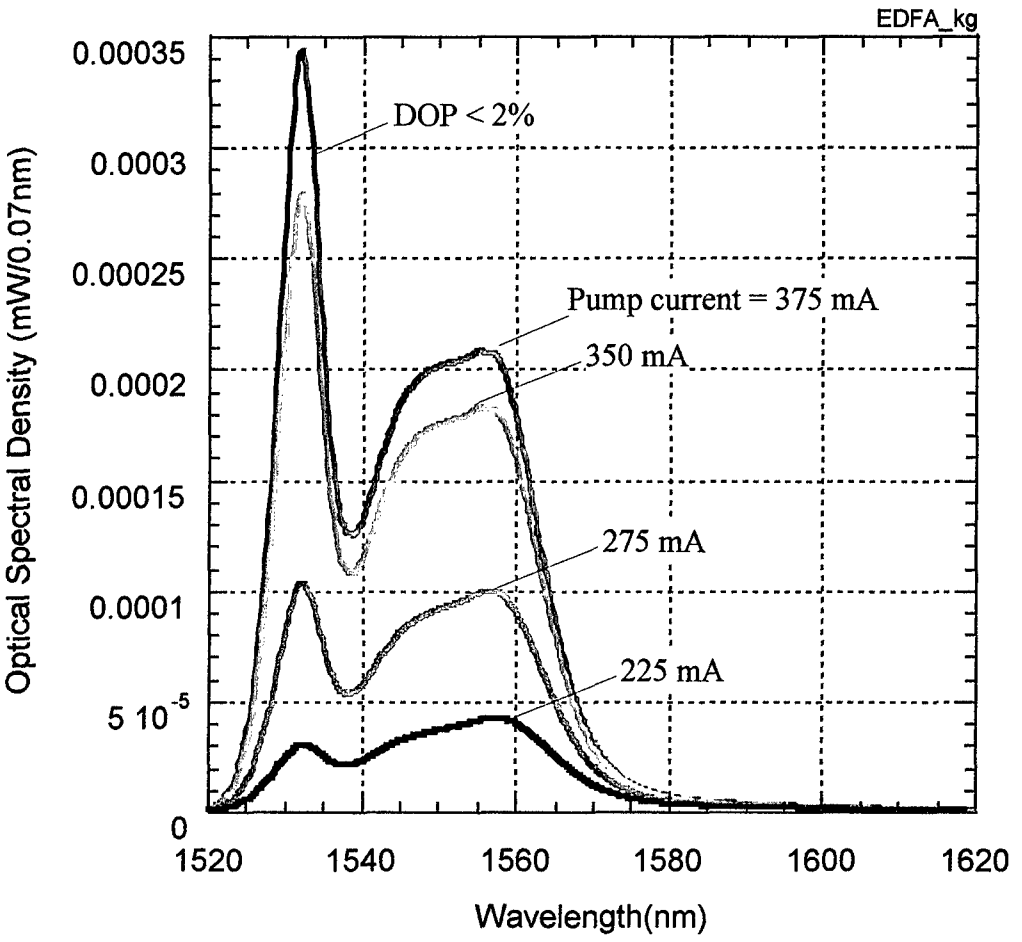

Fig. 4. *ASE spectrum of the EDFA amplifier at various pump current values. The degree of polarization (DOP) is indicated for the highest pump current curve.*

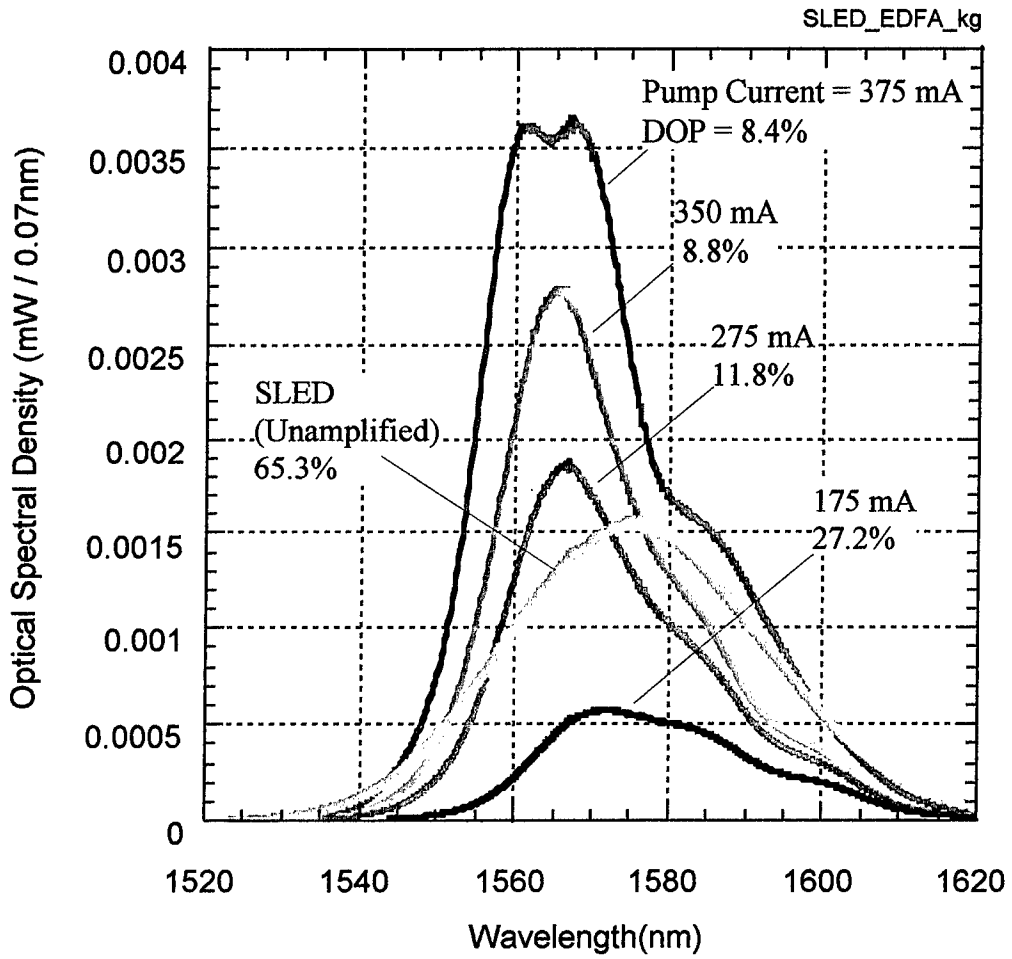

Fig. 5. *Optical spectrum of the SLED source after amplification by the EDFA comprising the ASE source for various pump current values. Degree-of-polarization (DOP) is also shown.*

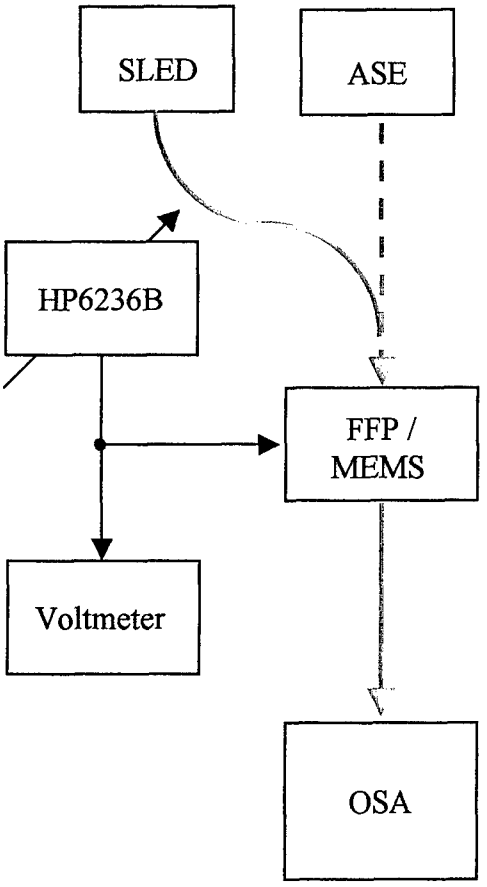

Fig. 6. *Experimental set-up for measuring voltage tuning characteristics of the filters. HP6236B = adjustable dc voltage, SLED = superluminescent LED, ASE = EDFA amplifier used as ASE source, OSA = optical spectrum analyzer.*

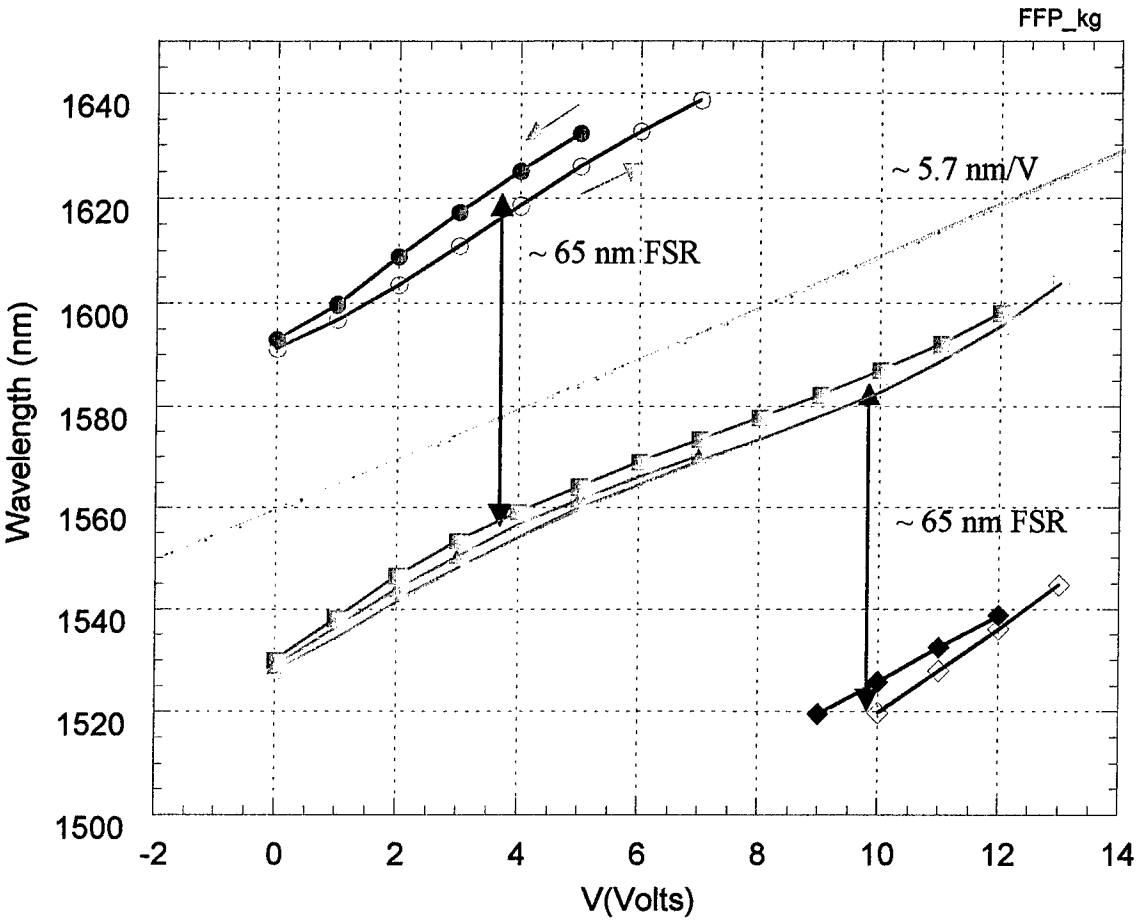

Fig. 7. *Voltage tuning characteristics of the FFP filter. Open symbols (increasing voltage), closed symbols (decreasing voltage).*

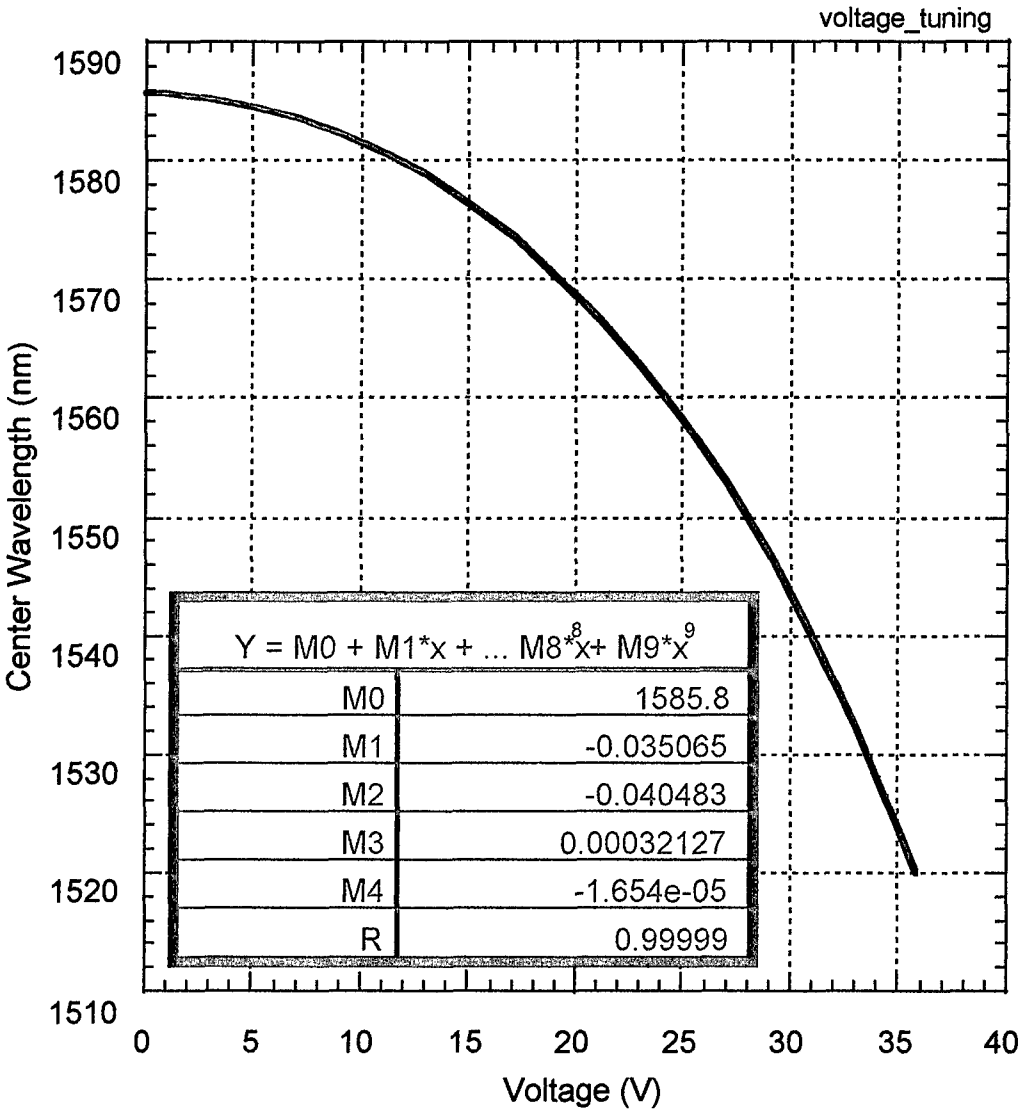

Fig. 8. *Voltage tuning characteristics of the MEMS filter.*

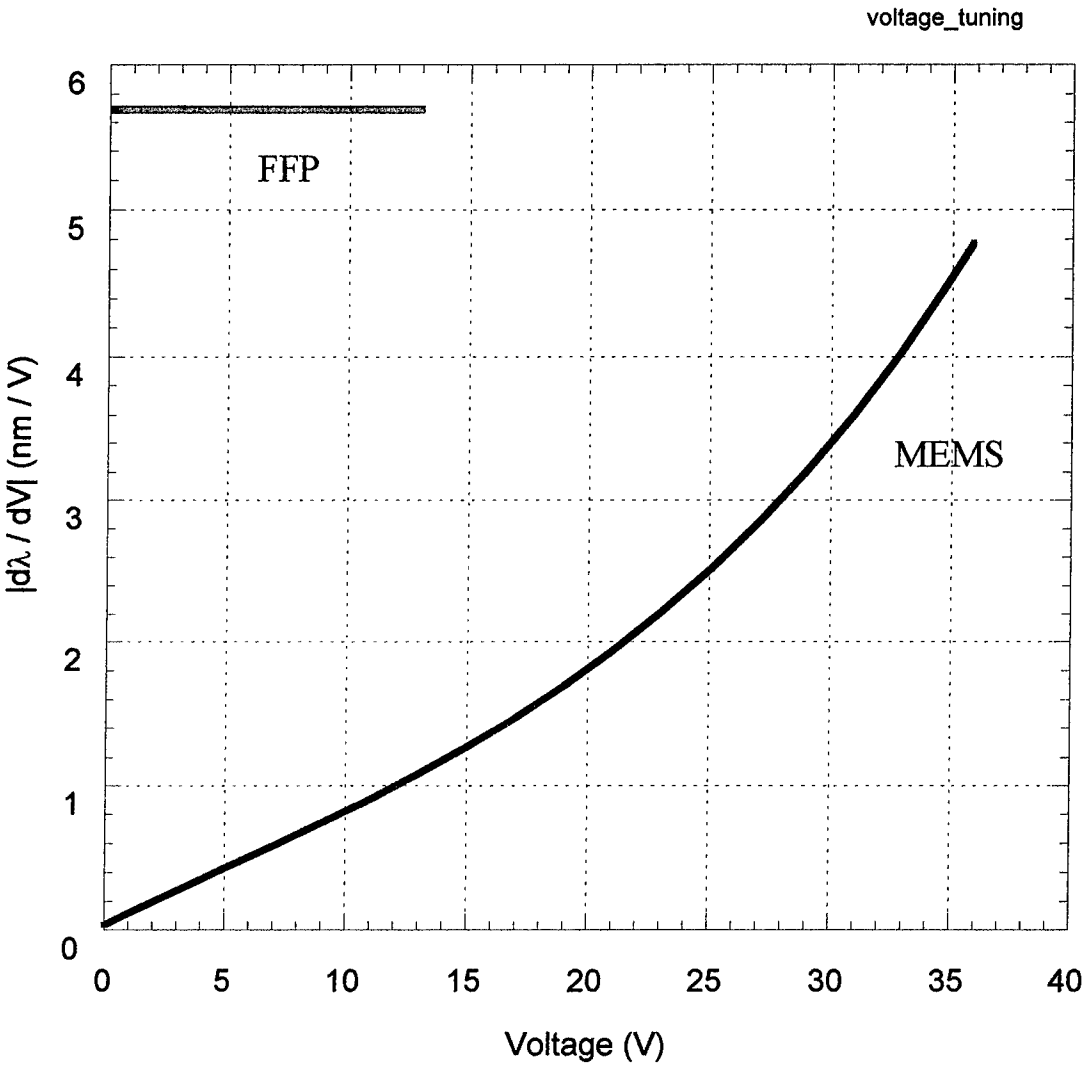

Fig. 9. *Comparison of the voltage tuning sensitivity of the FP and MEMS filters.*

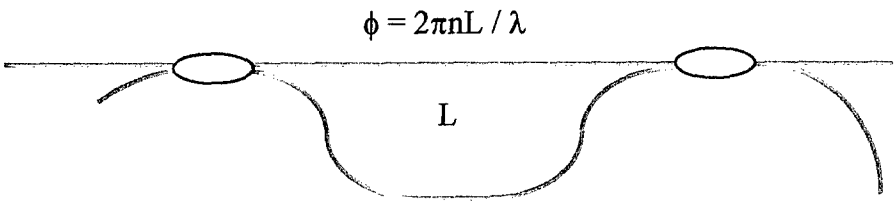

L = physical path imbalance

Fig. 10. *Fiber optic Mach-Zehnder interferometer having physical path imbalance L.*

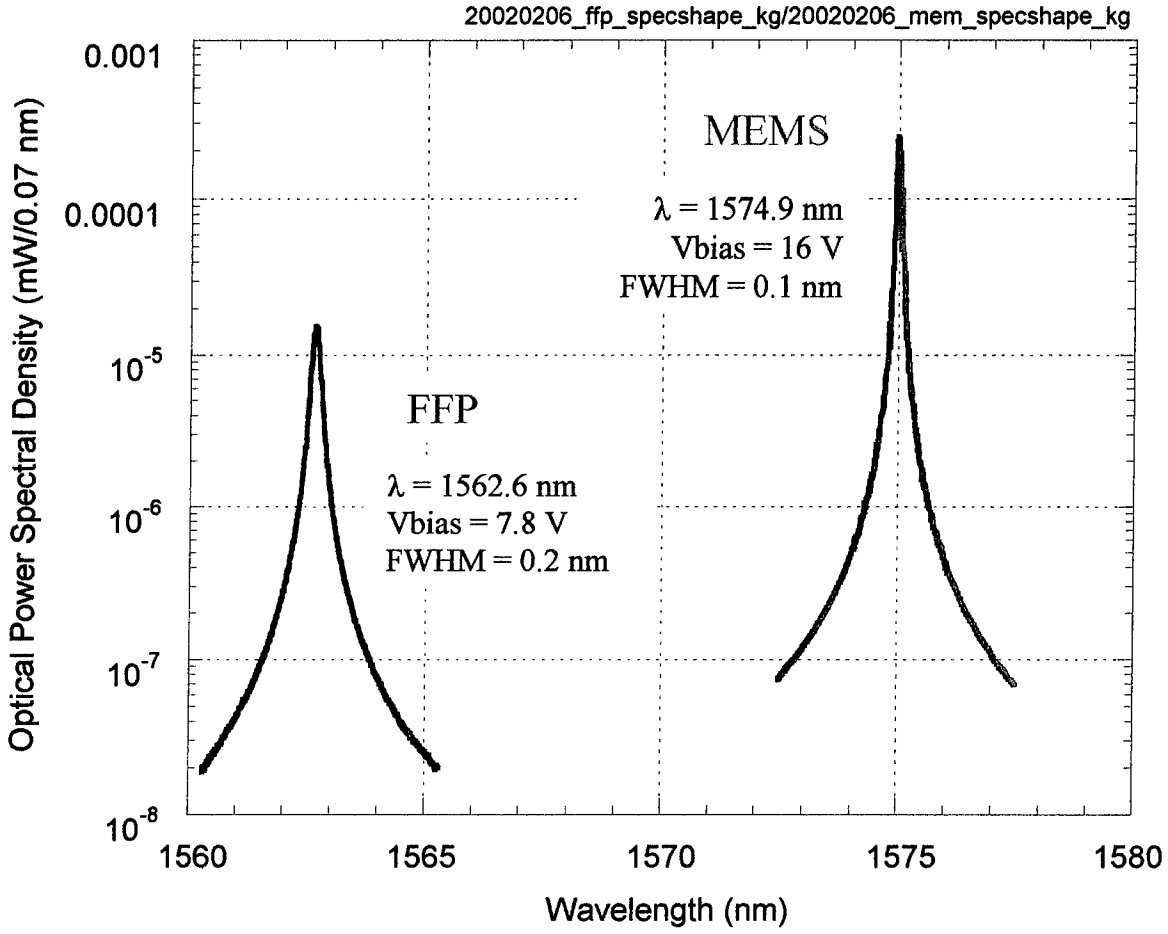

Fig. 11. *Normalized optical pass band of each filter. (Note: Reduced power for the FFP was due to the particular optical system in which the FFP was incorporated and is not indicative of a high insertion loss compared to the MEMS filter.)*

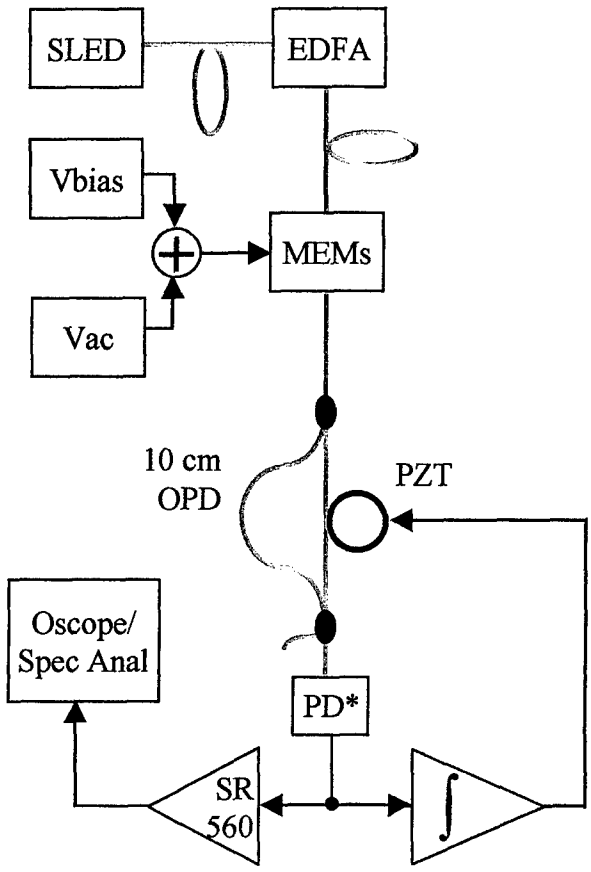

Fig. 12. *Interferometer system used to measure the small-signal frequency response. The interferometer was demodulated using active homodyne via a fiber-wound PZT cylinder in one arm of the interferometer.*

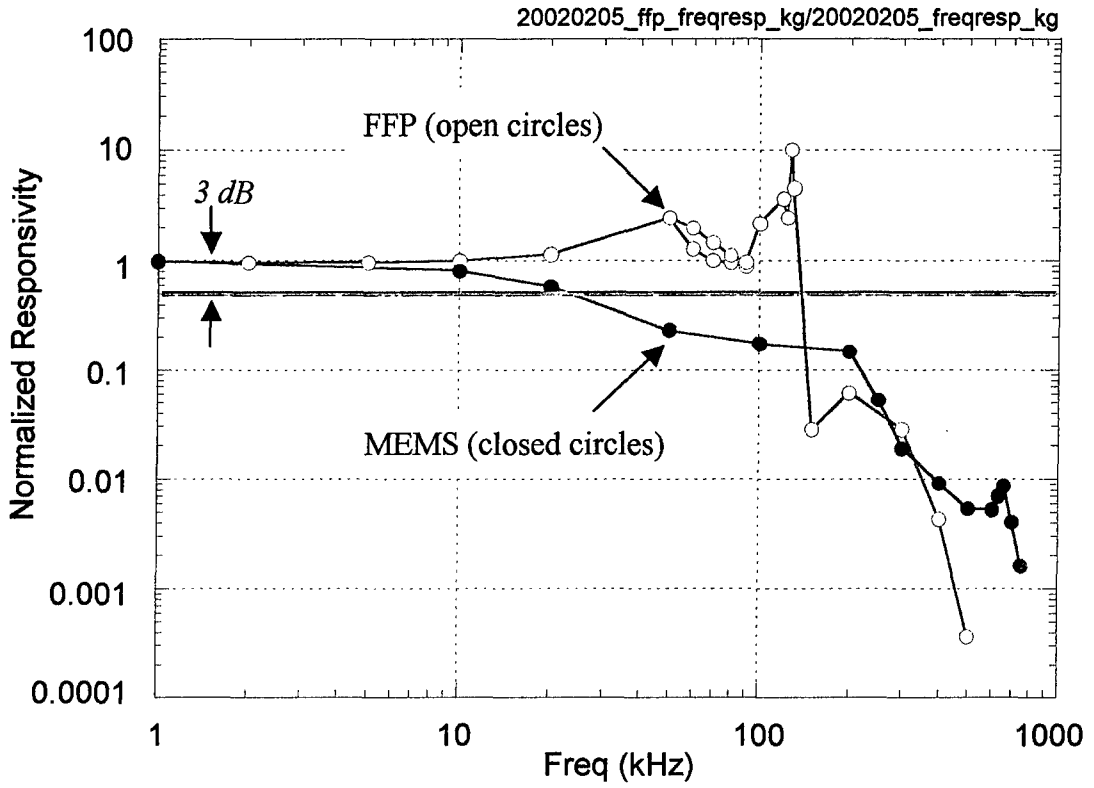

Fig. 13. *Small-signal frequency response of the two filters.*